

# Formation of bosonic $^{23}\text{Na}^{41}\text{K}$ Feshbach molecules

Sungjun Lee,<sup>\*</sup> Younghoon Lim,<sup>†</sup> \* Jongyeol Kim, Jaeryeong Chang, and Jee Woo Park<sup>‡</sup>  
*Department of Physics, Pohang University of Science and Technology, Pohang 37673, Republic of Korea*

Ultracold Feshbach molecules are a crucial intermediate step for the creation of quantum degenerate gases of strongly dipolar molecules. After coherent transfer to the rovibrational ground state, these dimers can realize stable dipolar gases with strong, tunable long-range interactions. Here, we report the creation of bosonic  $^{23}\text{Na}^{41}\text{K}$  Feshbach molecules by radio-frequency (RF) association. An RF pulse applied on the molecular side of an interspecies Feshbach resonance at 73.6(1) G associates up to  $1.1(1) \times 10^4$  molecules from a thermal mixture of  $^{23}\text{Na}$  and  $^{41}\text{K}$  atoms. Measurements of the binding energy reveal a broad resonance width of 5.1(2) G, facilitating robust control over interspecies interactions. The molecule lifetime in the presence of background atoms exceeds 2 ms, extending to 7 ms after removal of  $^{23}\text{Na}$ . These results constitute a key step toward the production of ultracold  $^{23}\text{Na}^{41}\text{K}$  ground state molecules for the exploration of novel many-body phenomena in strongly dipolar Bose gases.

## I. INTRODUCTION

Ultracold dipolar molecules have emerged as a powerful platform for quantum science and technology [1, 2]. Their large electric dipole moments generate strong, tunable, and anisotropic long-range interactions, granting access to many-body phenomena beyond the reach of contact interactions, including dipolar crystals [3], quantum spin liquids [4], and the quantum simulation of extended Hubbard and lattice spin models [5, 6]. Leveraging their rich internal structure of vibrational, rotational, and hyperfine states, dipolar molecules support dipole-mediated quantum information protocols [7–9] and provide exquisite sensitivity for precision tests of fundamental symmetries and physics beyond the Standard Model [10].

The creation of stable, quantum degenerate gases of ground state molecules is the starting point for many of these applications. The established route proceeds by associating weakly bound bialkali dimers near an interspecies Feshbach resonance, followed by coherent transfer to the rovibrational ground state via stimulated Raman adiabatic passage (STIRAP). Since the first creation of fermionic  $^{40}\text{K}^{87}\text{Rb}$  molecules [11, 12], this approach has been successfully applied to an expanding range of bialkali species [13–22]. Advances in atomic and molecular control have enabled the creation of a quantum degenerate Fermi gas of  $^{40}\text{K}^{87}\text{Rb}$  molecules [23], while techniques of dipolar shielding and molecular evaporative cooling have led to the realization of a degenerate Fermi gas of  $^{23}\text{Na}^{40}\text{K}$  [24] and molecular Bose-Einstein condensates of  $^{23}\text{Na}^{133}\text{Cs}$  [25] and  $^{23}\text{Na}^{87}\text{Rb}$  [26].

Among experimentally realized bialkali molecules, NaK offers several notable advantages. Its large electric dipole moment of 2.72 D [27] provides stronger dipolar interactions than in most other bialkali molecules. Ground

state NaK is also stable against exothermic exchange reactions, suppressing two-body losses and enhancing the stability of the molecular gas [15, 28]. Furthermore, NaK offers both bosonic and fermionic isotopologues, allowing the exploration of bosonic and fermionic dipolar many-body phenomena as well as comparative studies of quantum statistics in ultracold chemical reactions [29, 30]. For the bosonic isotopologues,  $^{23}\text{Na}^{41}\text{K}$  is particularly promising, as favorable inter- and intraspecies scattering lengths have enabled the creation of large, ultracold atomic mixtures of  $^{23}\text{Na}$  and  $^{41}\text{K}$  [31], providing an ideal starting point for the realization of high phase space density molecular gases.

In this Article, we report the creation of ultracold gases of weakly bound  $^{23}\text{Na}^{41}\text{K}$  bosonic Feshbach molecules. A radio-frequency (RF) pulse applied on the molecular side of an interspecies *s*-wave Feshbach resonance at 73.6(1) G associates over  $10^4$  dimers from a  $^{23}\text{Na}$ - $^{41}\text{K}$  mixture at temperatures as low as 170 nK. The corresponding phase space density of the molecular gas is estimated to be 0.03(1). RF spectroscopy maps the molecular binding energy versus magnetic field, precisely characterizing the Feshbach resonance and revealing a broad width of 5.1(2) G. Near threshold, we systematically explore the association efficiency as a function of temperature, pulse duration, and atom number ratio. We then employ an extended rate-equation model [32], modified to include molecular losses from collisions with both  $^{23}\text{Na}$  and  $^{41}\text{K}$ , to interpret the observed association dynamics. Remarkably, this extended model, with parameters constrained solely by the association efficiency measurements, quantitatively reproduces the measured lifetimes. We observe molecular lifetimes exceeding 2 ms over a range of binding energies, extending to 7 ms after removal of  $^{23}\text{Na}$ . These results demonstrate that high phase space density samples of  $^{23}\text{Na}^{41}\text{K}$  Feshbach molecules can be produced and quantitatively characterized, providing an excellent starting point for creating ultracold gases of ground state  $^{23}\text{Na}^{41}\text{K}$  molecules.

<sup>\*</sup> These authors contributed equally.

<sup>†</sup> Current address: 3rd R&D Institute, Agency for Defense Development, Daejeon 34186, Republic of Korea

<sup>‡</sup> jeewoopark@postech.ac.kr

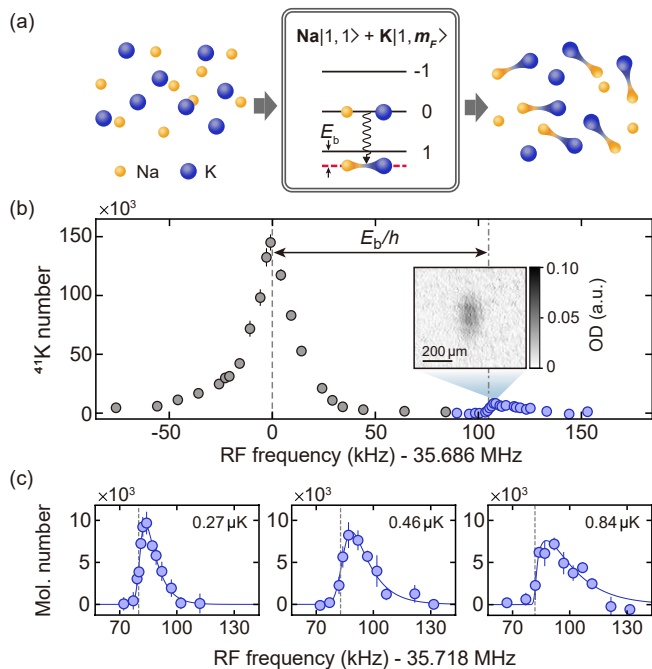


FIG. 1. Formation of bosonic  $^{23}\text{Na}^{41}\text{K}$  Feshbach molecules. (a) Schematic illustration of RF association from free atoms to weakly bound Feshbach molecules. (b) Arrival spectroscopy of Feshbach molecules at  $B=72.3$  G. Gray circles show the number of  $^{41}\text{K}$   $|1,1\rangle$  atoms; the dashed line marks the atomic spin-flip transition at 35.686(1) MHz. Blue circles show the associated molecule number; the dash-dotted line indicates the fitted molecular resonance at 35.791(1) MHz. The inset shows an absorption image of molecules taken in trap on the  $^{41}\text{K}$  imaging transition. (c) Number of associated molecules versus RF frequency at  $B=72.4$  G for mixture temperatures of 0.26(10)  $\mu\text{K}$ , 0.43(21)  $\mu\text{K}$ , and 0.73(6)  $\mu\text{K}$ . Fits to the asymmetric free-to-bound lineshape yield temperatures of 0.27(3)  $\mu\text{K}$ , 0.46(6)  $\mu\text{K}$ , and 0.84(12)  $\mu\text{K}$ , respectively. Error bars denote the standard error of the mean.

## II. RESULTS

### A. Sample preparation

The experiment begins by preparing ultracold mixtures of  $^{23}\text{Na}$  and  $^{41}\text{K}$ , as described in Refs. [31, 33]. For the work presented here, the atoms are confined in an oblate, single-beam 1064 nm optical dipole trap (ODT) in the  $|F, m_F\rangle = ^{23}\text{Na}|1,1\rangle + ^{41}\text{K}|1,1\rangle$  hyperfine state combination, where  $F$  and  $m_F$  denote the total angular momentum and its projection. After evaporative cooling in the ODT, the mixture contains approximately  $N_{\text{Na}} = 1\text{--}1.5 \times 10^5$  sodium and  $N_{\text{K}} = 2.5\text{--}4 \times 10^5$  potassium atoms at temperatures between 1.2 and 0.2  $\mu\text{K}$ . At the lowest temperature, the trapping frequencies for sodium are  $\{\omega_x, \omega_y, \omega_z\}_{\text{Na}} = 2\pi \times \{18(1), 8(1), 703(16)\}$  Hz. The atom number ratio and temperature are controlled by varying the number of  $^{41}\text{K}$  atoms captured in the magnetic trap and by adjusting the final ODT depth at the

end of evaporative cooling.

To access the interspecies Feshbach resonance previously identified near 73 G for the  $^{23}\text{Na}|1,1\rangle + ^{41}\text{K}|1,1\rangle$  collision channel [31], the magnetic field is first ramped to 40 G. Here, the differential Zeeman splitting between the  $|1,1\rangle \rightarrow |1,0\rangle$  transitions of  $^{23}\text{Na}$  and  $^{41}\text{K}$  is sufficiently large to selectively transfer  $^{41}\text{K}$  atoms to the spectator  $|1,0\rangle$  state via a Landau-Zener (LZ) sweep. Then, the magnetic field is ramped to a final value  $B$  on the molecular side of the resonance to perform RF association (see “Methods” for the details of the experimental sequence).

### B. RF association of Feshbach molecules

Feshbach molecules are created by using RF photons to coherently couple pairs of colliding atoms to a weakly bound molecular state near a Feshbach resonance. Starting from the  $^{23}\text{Na}|1,1\rangle + ^{41}\text{K}|1,0\rangle$  mixture at magnetic field  $B$ , we apply an RF pulse that drives the  $|1,0\rangle \rightarrow |1,1\rangle$  transition of  $^{41}\text{K}$ . When the RF frequency is detuned by  $E_b/h$  from the atomic transition, where  $E_b$  is the molecular binding energy and  $h$  is the Planck constant, the RF field transfers atom pairs into the least-bound molecular state associated with the  $^{23}\text{Na}|1,1\rangle + ^{41}\text{K}|1,1\rangle$  threshold (see Fig. 1(a)).

Figure 1(b) shows a representative RF spectrum recorded at  $B = 72.3$  G. To probe the molecular bound state, we apply a Blackman-shaped RF pulse with a duration of 3.15 ms and Rabi coupling  $\Omega = 2\pi \times 9.3$  kHz, followed by absorption imaging of  $^{41}\text{K}$  in the  $|1,1\rangle$  hyperfine state. Although weakly bound dimers near threshold can, in principle, be imaged using their constituent atomic transitions, at fields near 73 G neither  $^{23}\text{Na}$  nor  $^{41}\text{K}$  in  $|1,1\rangle$  possesses a closed optical cycling transition. We therefore implement a repumping scheme on  $^{41}\text{K}$  to maintain population in a bright manifold of hyperfine states during imaging, which enhances the observed signal by approximately a factor of two (see “Methods” for the details on imaging Feshbach molecules).

Scanning the RF frequency reveals two distinct features corresponding to the atomic spin-flip and molecule association [Fig. 1(b)]. The molecular peak exhibits a pronounced asymmetry, which arises from the thermal distribution of relative kinetic energies among the colliding atom pairs. To accurately extract the binding energy from the separation between these two features, we fit the molecular spectrum using a free-to-bound transition model that accounts for the phase-space overlap of the mixture (see “Methods” for the fitting model). This yields a binding energy of  $E_b/h = 105(1)$  kHz at  $B = 72.3$  G. As this model explicitly accounts for the collision energy distribution, we can also extract the sample temperature from the asymmetric free-to-bound lineshape. Figure 1(c) shows association spectra at  $B = 72.4$  G for varied temperatures. The fitted temperatures agree well with independent time-of-flight measurements, and the binding energies extracted from these fits,

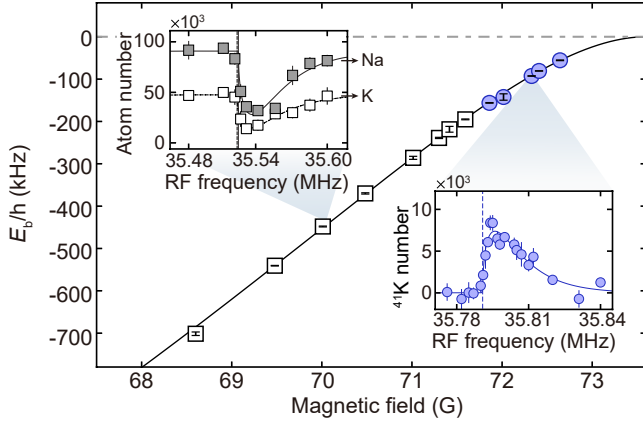


FIG. 2. Molecular binding energy versus magnetic field. Blue circles and white squares denote measurements from arrival spectroscopy and atom-loss spectroscopy, respectively. The solid line is a fit to the asymptotic binding energy model weighted by errors. The lower right inset shows the arrival spectrum at  $B = 72.3$  G, yielding  $E_b/h = 105(1)$  kHz. The upper left inset shows representative atom-loss spectra for Na (gray squares) and K (white squares), giving  $E_b/h = 448(1)$  kHz. Error bars denote the standard error of the mean.

$E_b/h = 81(1)$  kHz, remain consistent across the temperature range.

Since absorption imaging becomes inefficient for more deeply bound molecules, we determine the binding energy in this regime using atom-loss spectroscopy. To this end, we apply a 200 ms square RF pulse to the atomic mixture, during which Feshbach molecules are formed and subsequently lost from the trap through inelastic collisions with background atoms. We then image the remaining  $^{23}\text{Na}$  and  $^{41}\text{K}$  atoms to obtain a loss spectrum, as shown in the upper inset of Fig. 2. By combining arrival and loss measurements, we map out the molecular binding energy over a broad range of magnetic fields [Fig. 2].

We fit the measured binding energies with the universal expression  $E_b(B) = \hbar^2 / [2\mu(a(B) - \bar{a})^2]$ , where  $a(B) = a_{\text{bg}}[1 - \Delta/(B - B_0)]$  [34]. Here,  $a(B)$  is the inter-species scattering length,  $\bar{a} = 51.1a_0$  is the mean scattering length fixed by the van der Waals coefficient of NaK [35],  $a_{\text{bg}}$  is the background scattering length,  $B_0$  and  $\Delta$  are the resonance position and width, and  $\mu$  is the reduced mass of the atom pair. The fit yields  $B_0 = 73.6(1)$  G,  $\Delta = 5.1(2)$  G, and  $a_{\text{bg}} = 235(3)a_0$ , in good agreement with coupled-channel calculations [36]. For comparison, the singlet and triplet background scattering lengths have been predicted to be  $a_s = -3.65a_0$  and  $a_t = 267a_0$ , respectively. Importantly, the broad width of this low-field resonance provides a robust and convenient handle for tuning the interspecies interactions over a wide range in our experiments.

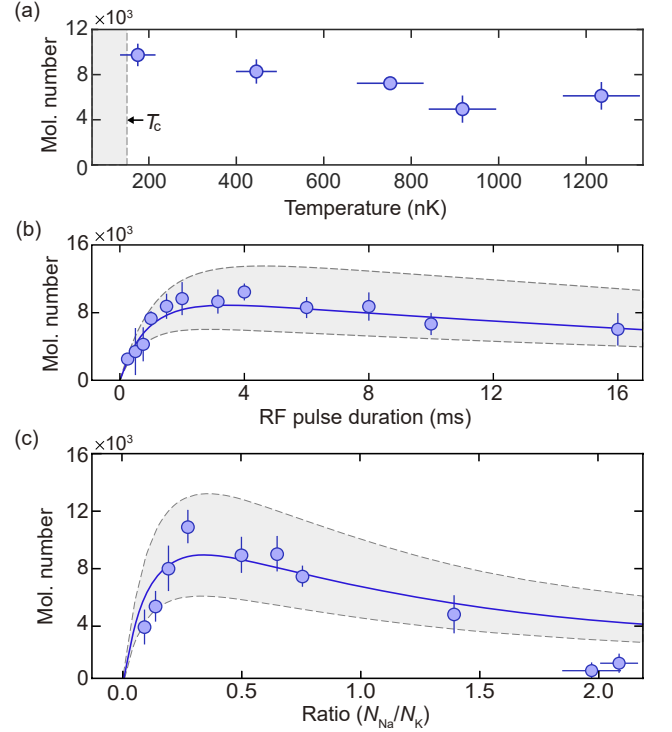


FIG. 3. Characterization of molecule association. (a) Number of molecules as a function of temperature. The gray-shaded area indicates the temperature range below the critical temperature of  $^{41}\text{K}$ . The temperatures are extracted from the thermal wings of the  $^{41}\text{K}$  clouds. (b) Molecule number versus RF pulse duration. The maximum number is reached near  $\sim 3.4$  ms, after which the loss becomes dominant over the molecule association. (c) Number of molecules created at various mixture ratios. To ensure an adequate dynamic range for these measurements, the typical temperature is kept at  $\sim 0.5$   $\mu\text{K}$ . The solid lines represent numerical solutions of the rate equations fitted to the experimental data. The dashed lines are  $\pm 1\sigma$  confidence intervals, and the error bars denote the standard error of the mean.

### C. Characterization of molecule association

To optimize the molecule-creation efficiency, we characterize the association process as a function of temperature, RF pulse duration, and atom number ratio. The optimization is performed near the threshold, where the association efficiency depends only weakly on the molecular binding energy. First, we examine the temperature dependence of the molecule number, as shown in Fig. 3(a). By adjusting the ODT depth at the end of evaporation, we tune the temperature between 1.2  $\mu\text{K}$  and 0.2  $\mu\text{K}$ , while keeping the atom number ratio fixed. Although the total atom number decreases as evaporation proceeds to lower temperatures, the molecular yield increases due to improved phase space overlap between the two species. The differential gravitational sag between  $^{23}\text{Na}$  and  $^{41}\text{K}$  is about 0.15  $\mu\text{m}$ , which is negligible compared to the sample size along the gravitational direction, 1.3  $\mu\text{m}$ . At

the lowest temperatures, we infer a peak molecular phase space density of 0.03(1), assuming that the molecules are thermalized to the mixture temperature. However, below 150 nK, no Feshbach molecules are detected in the absorption images. We attribute this disappearance to the onset of  $^{41}\text{K}$  Bose-Einstein condensation, which strongly enhances inelastic molecular loss due to the high atomic density.

The dependence of the molecule number on RF pulse duration and mixture ratio further reflects a competition between association and inelastic loss due to collisions with residual atoms. To facilitate a quantitative analysis of these kinetics, we employ square RF pulses of constant amplitude rather than the Blackman pulses used for spectroscopy, ensuring a time-independent association rate that simplifies the modeling. The resulting molecular yields are shown in Fig. 3(b) and (c), where we vary the RF pulse duration at fixed atom number ratio and the atom number ratio at fixed pulse duration, respectively. To interpret these observations, we use a rate-equation model adapted from Ref. [32] and extend it to distinguish between molecule loss channels driven by collisions with  $^{23}\text{Na}$  and  $^{41}\text{K}$ . The dynamics are described by coupled equations for the molecular population  $N_{\text{mol}}$  and the atomic populations  $N_{\text{Na}}$  and  $N_{\text{K}}$ :

$$\begin{aligned} \frac{dN_{\text{mol}}}{dt} &= +k_{\text{mol}}g_{\text{Na,K}}N_{\text{Na}}N_{\text{K}} - \Gamma_{\text{Na}}g_{\text{mol,Na}}N_{\text{mol}}N_{\text{Na}} \\ &\quad - \Gamma_{\text{K}}g_{\text{mol,K}}N_{\text{mol}}N_{\text{K}} \\ \frac{dN_{\text{Na}}}{dt} &= -k_{\text{mol}}g_{\text{Na,K}}N_{\text{Na}}N_{\text{K}} - \Gamma_{\text{Na}}g_{\text{mol,Na}}N_{\text{mol}}N_{\text{Na}} \\ \frac{dN_{\text{K}}}{dt} &= -k_{\text{mol}}g_{\text{Na,K}}N_{\text{Na}}N_{\text{K}} - \Gamma_{\text{K}}g_{\text{mol,K}}N_{\text{mol}}N_{\text{K}} \end{aligned} \quad (1)$$

Here,  $k_{\text{mol}}$  is the molecule association coefficient, which depends on the RF pulse parameters, while  $\Gamma_{\text{Na}}$  and  $\Gamma_{\text{K}}$  are two-body inelastic loss coefficients for Na-NaK and K-NaK collisions, respectively. The geometric overlap factors  $g_{i,j} = \int n_i(\vec{r})n_j(\vec{r})d^3r/N_iN_j$  account for spatial mode matching and are evaluated assuming Gaussian density profiles determined by the known trap parameters.

We fit the solutions of Eq. (1) simultaneously to the measured molecule numbers as functions of pulse duration [Fig. 3(b)] and atom number ratio [Fig. 3(c)]. The model parameters are optimized by minimizing the combined least-squares error, yielding  $k_{\text{mol}} = 1.3(2) \times 10^{-10} \text{ cm}^3/\text{s}$ ,  $\Gamma_{\text{Na}} = 3.3(7) \times 10^{-9} \text{ cm}^3/\text{s}$ , and  $\Gamma_{\text{K}} = 7.4(43) \times 10^{-11} \text{ cm}^3/\text{s}$ . The model reproduces the observed data well and shows that the inelastic loss coefficient for Na-NaK collisions is about 45 times larger than that for K-NaK collisions, consistent with the resonant character of the collisions involving  $^{23}\text{Na}$  near the Feshbach resonance. The maximum molecule number,  $N_{\text{mol}} = 1.1(1) \times 10^4$ , occurs at an optimal atom number ratio of  $N_{\text{Na}}/N_{\text{K}} \approx 0.27$ . For larger ratios ( $N_{\text{Na}}/N_{\text{K}} \gtrsim 1.5$ ), the data begins to deviate from the model prediction. This discrepancy suggests the onset of higher-order loss processes not included in our two-body description,

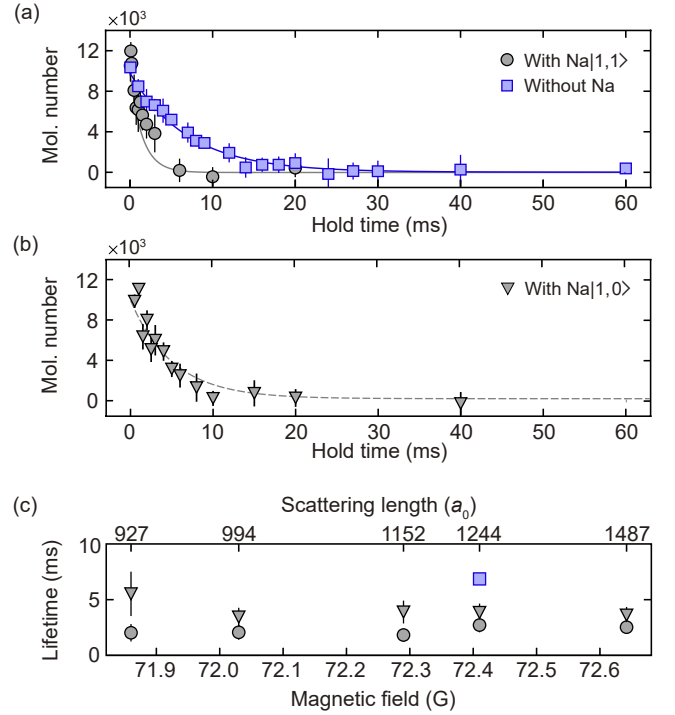


FIG. 4. Lifetime measurement of  $^{23}\text{Na}^{41}\text{K}$  Feshbach molecules. (a) Gray circles show the number of molecules as a function of hold time with  $^{23}\text{Na}$  prepared in the  $|1,1\rangle$  state. Blue squares show the number of molecules with  $^{23}\text{Na}$  removed. The solid lines are simulations obtained from the rate-equation model using the extracted loss coefficients. (b) Molecular lifetime with  $^{23}\text{Na}$  atoms transferred to the  $|1,0\rangle$  state. Error bars in (a) and (b) represent the standard error of the mean. (c) Measured molecular lifetimes as a function of magnetic field. The error bars of the lifetimes represent 95% confidence intervals.

such as three-body recombination involving two sodium atoms that become increasingly significant at high  $^{23}\text{Na}$  densities.

#### D. Molecular lifetimes

Understanding the collisional stability of  $^{23}\text{Na}^{41}\text{K}$  Feshbach molecules is essential for efficient transfer to the rovibrational ground state. We therefore measure their lifetime in the presence and absence of background  $^{23}\text{Na}$  atoms, which dominate the inelastic loss. With  $^{23}\text{Na}$  present, the  $1/e$  lifetime of the molecular gas is 2.1(8) ms [Fig. 4(a)]. To selectively remove the residual  $^{23}\text{Na}$  atoms without significantly affecting the Feshbach molecules, we transfer the sodium atoms to the  $|1,0\rangle$  state using a 120  $\mu\text{s}$  RF LZ sweep, followed by a 30  $\mu\text{s}$  resonant optical clean-out pulse. After this purification, the  $1/e$  lifetime extends to 6.9(10) ms.

The solid curves in Fig. 4(a) are parameter-free simulations of the molecular lifetimes rather than fits. They are obtained by numerically integrating the coupled rate

equations using the association and loss coefficients  $k_{\text{mol}}$ ,  $\Gamma_{\text{Na}}$ , and  $\Gamma_{\text{K}}$  independently determined from the association efficiency analysis. The simulations incorporate both molecule formation and loss during the 3.15 ms association pulse, followed by purely inelastic decay after the RF field is switched off. The excellent agreement between the measured data and these simulations quantitatively validates the coupled rate-equation model and confirms that the extracted rate coefficients are predictive across different experimental conditions.

We also measure the molecular lifetime when background  $^{23}\text{Na}$  is prepared in the spectator  $|1,0\rangle$  state [Fig. 4(b)], obtaining a  $1/e$  lifetime of 3.8(2) ms. Fitting the model to these data yields a Na-NaK loss coefficient of  $3.5(12) \times 10^{-10} \text{ cm}^3/\text{s}$ , roughly an order of magnitude smaller than in the resonant  $|1,1\rangle$  state. We further observe that these lifetimes remain nearly constant across the experimentally accessed magnetic field range [Fig. 4(c)]. This weak dependence on the scattering length reflects the broad, open-channel dominated nature of the resonance.

Notably, the observed 6.9(10) ms lifetime is more than an order of magnitude longer than that reported for bosonic  $^{23}\text{Na}^{39}\text{K}$  Feshbach molecules [32]. We expect this lifetime to be further extended by removing the remaining  $^{41}\text{K}$  atoms [37]. This enhanced stability, combined with the fact that typical STIRAP transfer times are on the order of 20–100  $\mu\text{s}$ , provides a robust platform for the production of  $^{23}\text{Na}^{41}\text{K}$  ground state molecules.

### III. CONCLUSION

In conclusion, we have demonstrated the RF association of ultracold bosonic  $^{23}\text{Na}^{41}\text{K}$  Feshbach molecules. We have precisely characterized the key interspecies Feshbach resonance, determining a resonance position of  $B_0 = 73.6(1) \text{ G}$  and a width of  $\Delta = 5.1(2) \text{ G}$ , consistent with its broad, open-channel dominated character. Through optimized association, we produce over  $10^4$  molecules with an estimated phase space density of 0.03(1) and have performed a detailed characterization of their inelastic collision dynamics.

Our quantitative analysis highlights the predictive power of the extended rate-equation model. Using collision parameters constrained solely by the association efficiency measurements, the model accurately predicts the observed molecular lifetimes. We observe a lifetime of 2.1(8) ms in the presence of background atoms, which extends to 6.9(10) ms upon the removal of resonant  $^{23}\text{Na}$ . This timescale is sufficiently long to support robust STIRAP transfer to the rovibrational ground state.

These results establish  $^{23}\text{Na}^{41}\text{K}$  as a highly promising system for the production of ground state bosonic dipolar molecules. Combined with the creation of fermionic  $^{23}\text{Na}^{40}\text{K}$  molecules within the same experimental apparatus [33], this work further establishes NaK as a versatile platform for complementary studies of bosonic and

fermionic dipolar physics. Our results pave the way for the exploration of novel pairing mechanisms in multilayer dipolar Bose gases [38–40] and for quantum simulation of the extended Bose-Hubbard model in the regime of strong dipolar interactions, whose rich phase diagram includes exotic density-ordered phases not present in the standard Hubbard model [41].

## METHODS

### Experimental sequence

To prepare ultracold mixtures of  $^{23}\text{Na}$  and  $^{41}\text{K}$ ,  $^{23}\text{Na}$  atoms from a Zeeman slower and  $^{41}\text{K}$  atoms from a  $2\text{D}^+$  MOT are sequentially captured in a 3D MOT and optically pumped into their stretched  $|2,2\rangle$  states. Both species are then transferred into an optically plugged magnetic trap, where RF-induced evaporative cooling of  $^{23}\text{Na}$  sympathetically cools  $^{41}\text{K}$ . After RF evaporation, the mixture reaches a temperature of 11.2(1)  $\mu\text{K}$ , with  $N_{\text{Na}} = 1.7(1) \times 10^7$  and  $N_{\text{K}} = 1.1(1) \times 10^7$ .

The sample is subsequently loaded into a single-beam 1064 nm ODT for final evaporative cooling. At a bias field of 2 G, the atoms are transferred to the  $|1,1\rangle$  state via RF LZ sweeps with 150 ms duration to suppress dipolar and spin-exchange inelastic collisions. To selectively prepare  $^{41}\text{K}$  atoms in the  $|1,0\rangle$  state, the magnetic field is rapidly ramped to an intermediate value of 40 G within 1 ms. At this field, the differential Zeeman splitting between the  $|1,1\rangle \rightarrow |1,0\rangle$  transitions of  $^{23}\text{Na}$  and  $^{41}\text{K}$  is approximately 3.7 MHz, which is sufficiently large for selective transfer of  $^{41}\text{K}$  to  $|1,0\rangle$ . After a short hold time for field stabilization, a 60 ms RF LZ sweep on the  $^{41}\text{K}$   $m_F$  transition is performed. Finally, the magnetic field is ramped to the target field  $B$  near the 73 G resonance in 15 ms and stabilized for 200 ms before RF association. A diagram of this final sequence is shown in Fig. 5.

### Imaging of Feshbach molecules

Feshbach molecules near threshold can be imaged using the atomic transition, as their binding energy is smaller than the atomic linewidth. However, standard absorption imaging of both  $^{23}\text{Na}$  and  $^{41}\text{K}$  is challenging at  $B \sim 73 \text{ G}$  regime. At this field, atoms in the electronic ground  $S_{1/2}$  state have not yet reached the hyperfine Paschen-Back regime, and neither  $\{F, m_F\}$  nor  $\{J, I, m_J, m_I\}$  constitutes a good set of quantum numbers. Here,  $J$  and  $I$  are the total electronic angular momentum and nuclear spin quantum numbers, respectively, and  $m_J$  and  $m_I$  denote their projections onto the quantization axis. Consequently, the  $|1,1\rangle$  state lacks a closed optical cycling transition.

To address this issue, we employ a repumping scheme similar to that described in Ref. [42]. Our scheme uses a  $\sigma^-$ -polarized imaging beam to drive the primary transi-

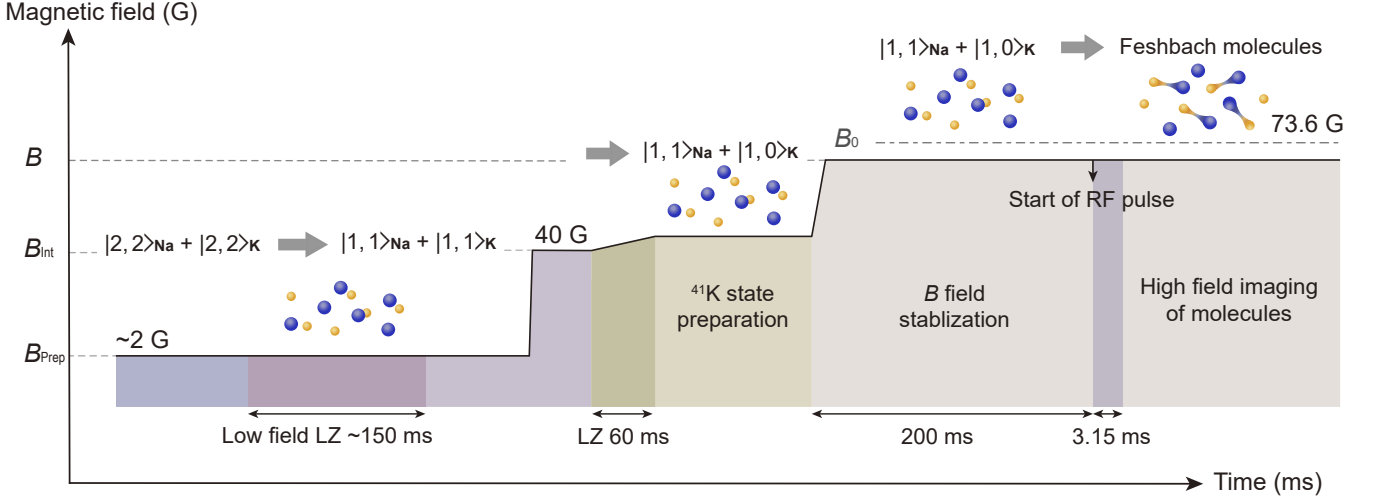


FIG. 5. Schematic diagram of the experimental sequence.  $B_{\text{prep}}$  denotes the magnetic field where the mixture is initially prepared before the ramp.  $B_{\text{int}}$  is the intermediate magnetic field for the LZ sweep of  $^{41}\text{K}$  atoms.  $B$  represents the magnetic field at which molecules are RF associated, set below the Feshbach resonance position  $B_0 = 73.6(1)$  G. The diagram is not to scale.

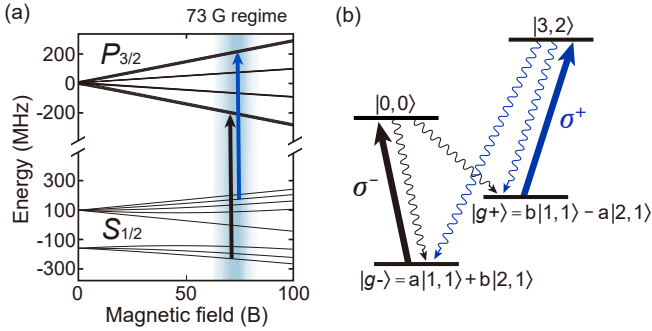


FIG. 6. (a) Hyperfine structure of the  $^2S_{1/2}$  ground state and the  $^2P_{3/2}$  excited state of  $^{41}\text{K}$ . The arrows in 73 G regime denote the  $\sigma^-$  imaging and  $\sigma^+$  repumping beams. (b) The diagram represents the corresponding repumping scheme. The amplitudes  $a \approx 0.974$  and  $b \approx 0.229$  are obtained via the hyperfine Zeeman effect at 73 G. Although the low-field  $|F, m_F\rangle$  states are not good quantum numbers, we use this basis to label the involved hyperfine components.

tion  $S_{1/2}|1, 1\rangle \rightarrow P_{3/2}|0, 0\rangle$  [Fig. 6]. During this process, excited atoms can spontaneously decay to a dark state, with dominant  $S_{1/2}|2, 1\rangle$  contribution. To close this leakage channel, we simultaneously apply a  $\sigma^+$ -polarized repumping beam, which excites atoms from the  $S_{1/2}|2, 1\rangle$  state to the  $P_{3/2}|3, 2\rangle$  state, allowing them to decay back to the  $S_{1/2}|1, 1\rangle$  state. Using this technique, the imaging efficiency of  $^{41}\text{K}$  atoms is increased from approximately 35% to 60%. The same scheme is used to image near-threshold Feshbach molecules.

### RF association lineshape model

In the measured molecular spectra, a simple Gaussian fit does not accurately extract the binding energies, as the lineshape is an asymmetric convolution of the thermal energy distribution and the RF pulse spectrum. Instead, we use a model based on a perturbative approach analogous to Fermi's golden rule [43, 44]. The number of associated molecules  $N_{\text{mol}}$  at a given RF frequency  $\nu$  and temperature  $T$  is obtained by integrating over the relative kinetic energy  $\epsilon_r$  of the unbound atom pairs:

$$N_{\text{mol}}(\nu, E_b, T) \propto \int_0^\infty d\epsilon_r F(\epsilon_r, E_b) h(\epsilon_r, T) |B(t_d, \omega)|^2 \quad (2)$$

Here,  $h(\epsilon_r, T)$  is the thermal distribution of free atom pairs available for association, given by the Boltzmann distribution  $h(\epsilon_r, T) = A(\bar{\omega}_i, T) \exp(-\epsilon_r/k_B T)$ , where  $A(\bar{\omega}_i, T)$  is a coefficient that depends on the mean trap frequency  $\bar{\omega}_i$ .  $F(\epsilon_r, E_b)$  is the Franck-Condon factor, which describes the spatial overlap between the initial free-atom wavefunction and the final bound molecular wavefunction, where  $E_b$  is the molecular binding energy. We use the simplified form  $F \sim \frac{2}{\pi} \epsilon_r^{1/2} E_b^{-3/2} (1 + \epsilon_r/E_b)^{-2}$ , which is valid in the universal limit [45].  $B(t_d, \omega)$  is the lineshape function given by the Fourier transform of the RF pulse. We use a Blackman pulse of duration  $t_d$  to suppress spectral sidelobes. The Fourier-transformed spectrum of this pulse profile is given by:

$$B(t_d, \omega) = \omega \sin \frac{\omega t_d}{2} \left( \frac{0.84}{\omega^2} - \frac{1}{\omega^2 - (2\pi/t_d)^2} + \frac{0.16}{\omega^2 - (4\pi/t_d)^2} \right) \quad (3)$$

where the detuning  $\omega$  is defined as  $\omega = 2\pi(\nu - \epsilon_r/h - \nu_A - E_b/h)$ . Here,  $\nu_A$  is the bare atomic transition frequency.



## ACKNOWLEDGEMENTS

This work was supported by the National Research Foundation of Korea (Grants No. RS-2025-00559423, RS-2025-02317602, RS-2023-NR119931), the Samsung Science and Technology Foundation (Project No. SSTF-BA2001-06), and the Ministry of Science and ICT, Korea,

under the ITRC support program (Grant No. RS-2022-00164799) supervised by the IITP. Y. Lim acknowledges the support from the NRF BK21 FOUR Postdoctoral Fellowship and S. Lee from the Hyundai Motor Chung Mong-Koo Foundation.

- 
- [1] L. D. Carr, D. DeMille, R. V. Krems, and J. Ye, Cold and ultracold molecules: science, technology and applications, *New J. Phys.* **11**, 055049 (2009).
  - [2] J. L. Bohn, A. M. Rey, and J. Ye, Cold molecules: Progress in quantum engineering of chemistry and quantum matter, *Science* **357**, 1002 (2017).
  - [3] H. P. Büchler, E. Demler, M. Lukin, A. Micheli, N. Prokof'ev, G. Pupillo, and P. Zoller, Strongly correlated 2D quantum phases with cold polar molecules: Controlling the shape of the interaction potential, *Phys. Rev. Lett.* **98**, 060404 (2007).
  - [4] N. Y. Yao, M. P. Zaletel, D. M. Stamper-Kurn, and A. Vishwanath, A quantum dipolar spin liquid, *Nat. Phys.* **14**, 405 (2018).
  - [5] B. Capogrosso-Sansone, C. Trefzger, M. Lewenstein, P. Zoller, and G. Pupillo, Quantum phases of cold polar molecules in 2D optical lattices, *Phys. Rev. Lett.* **104**, 125301 (2010).
  - [6] A. Micheli, G. K. Brennen, and P. Zoller, A toolbox for lattice-spin models with polar molecules, *Nat. Phys.* **2**, 341 (2006).
  - [7] D. DeMille, Quantum computation with trapped polar molecules, *Phys. Rev. Lett.* **88**, 067901 (2002).
  - [8] K.-K. Ni, T. Rosenband, and D. D. Grimes, Dipolar exchange quantum logic gate with polar molecules, *Chem. Sci.* **9**, 6830 (2018).
  - [9] L. R. B. Picard, A. J. Park, G. E. Patenotte, S. Gebretsadkan, D. Wellnitz, A. M. Rey, and K.-K. Ni, Entanglement and iswap gate between molecular qubits, *Nature* **637**, 821 (2025).
  - [10] D. DeMille, N. R. Hutzler, A. M. Rey, and T. Zelevinsky, Quantum sensing and metrology for fundamental physics with molecules, *Nat. Phys.* **20**, 741 (2024).
  - [11] J. J. Zirbel, K.-K. Ni, S. Ospelkaus, J. P. D'Incao, C. E. Wieman, J. Ye, and D. S. Jin, Collisional stability of fermionic feshbach molecules, *Phys. Rev. Lett.* **100**, 143201 (2008).
  - [12] K.-K. Ni, S. Ospelkaus, M. H. G. de Miranda, A. Pe'er, B. Neyenhuis, J. J. Zirbel, S. Kotochigova, P. S. Julienne, D. S. Jin, and J. Ye, A high phase-space-density gas of polar molecules, *Science* **322**, 231 (2008).
  - [13] T. Takekoshi, L. Reichsöllner, A. Schindewolf, J. M. Hutson, C. R. Le Sueur, O. Dulieu, F. Ferlaino, R. Grimm, and H.-C. Nägerl, Ultracold dense samples of dipolar RbCs molecules in the rovibrational and hyperfine ground state, *Phys. Rev. Lett.* **113**, 205301 (2014).
  - [14] P. K. Molony, P. D. Gregory, Z. Ji, B. Lu, M. P. Köppinger, C. R. Le Sueur, C. L. Blackley, J. M. Hutson, and S. L. Cornish, Creation of ultracold  $^{87}\text{Rb}^{133}\text{Cs}$  molecules in the rovibrational ground state, *Phys. Rev. Lett.* **113**, 255301 (2014).
  - [15] J. W. Park, S. A. Will, and M. W. Zwierlein, Ultracold dipolar gas of fermionic  $^{23}\text{Na}^{40}\text{K}$  molecules in their absolute ground state, *Phys. Rev. Lett.* **114**, 205302 (2015).
  - [16] M. Guo, B. Zhu, B. Lu, X. Ye, F. Wang, R. Vexiau, N. Bouloufa-Maafa, G. Quémener, O. Dulieu, and D. Wang, Creation of an ultracold gas of ground-state dipolar  $^{23}\text{Na}^{87}\text{Rb}$  molecules, *Phys. Rev. Lett.* **116**, 205303 (2016).
  - [17] T. M. Rvachov, H. Son, A. T. Sommer, S. Ebadi, J. J. Park, M. W. Zwierlein, W. Ketterle, and A. O. Jamison, Long-lived ultracold molecules with electric and magnetic dipole moments, *Phys. Rev. Lett.* **119**, 143001 (2017).
  - [18] K. K. Voges, P. Gersema, M. Meyer zum Alten Borgloh, T. A. Schulze, T. Hartmann, A. Zenesini, and S. Ospelkaus, Ultracold gas of bosonic  $^{23}\text{Na}^{39}\text{K}$  ground-state molecules, *Phys. Rev. Lett.* **125**, 083401 (2020).
  - [19] W. B. Cairncross, J. T. Zhang, L. R. B. Picard, Y. Yu, K. Wang, and K.-K. Ni, Assembly of a rovibrational ground state molecule in an optical tweezer, *Phys. Rev. Lett.* **126**, 123402 (2021).
  - [20] I. Stevenson, A. Z. Lam, N. Bigagli, C. Warner, W. Yuan, S. Zhang, and S. Will, Ultracold gas of dipolar NaCs ground state molecules, *Phys. Rev. Lett.* **130**, 113002 (2023).
  - [21] C. He, X. Nie, V. Avalos, S. Botsi, S. Kumar, A. Yang, and K. Dieckmann, Efficient creation of ultracold ground state  $^6\text{Li}^{40}\text{K}$  polar molecules, *Phys. Rev. Lett.* **132**, 243401 (2024).
  - [22] K. P. Zamariski, C. Beulenkamp, Y. Zeng, M. Landini, and H.-C. Nägerl, Spectroscopy and ground-state transfer of ultracold bosonic  $^{39}\text{K}^{133}\text{Cs}$  molecules, *Phys. Rev. Lett.* **135**, 203401 (2025).
  - [23] L. D. Marco, G. Valtolina, K. Matsuda, W. G. Tobias, J. P. Covey, and J. Ye, A degenerate fermi gas of polar molecules, *Science* **363**, 853 (2019).
  - [24] A. Schindewolf, R. Bause, X.-Y. Chen, M. Duda, T. Karman, I. Bloch, and X.-Y. Luo, Evaporation of microwave-shielded polar molecules to quantum degeneracy, *Nature* **607**, 677 (2022).
  - [25] N. Bigagli, W. Yuan, S. Zhang, B. Bulatovic, T. Karman, I. Stevenson, and S. Will, Observation of bose-einstein condensation of dipolar molecules, *Nature* **631**, 289 (2024).
  - [26] Z. Shi, Z. Huang, F. Deng, W.-J. Jin, S. Yi, T. Shi, and D. Wang, Bose-einstein condensate of ultracold sodium-rubidium molecules with tunable dipolar interactions (2025), arXiv:2508.20518.
  - [27] A. Gerdes, O. Dulieu, H. Knöckel, and E. Tiemann, Stark effect measurements on the NaK molecule, *Eur. Phys. J. D* **65**, 105 (2011).
  - [28] P. S. Żuchowski and J. M. Hutson, Reactions of ultracold alkali-metal dimers, *Phys. Rev. A* **81**, 060703 (2010).
  - [29] M.-G. Hu, Y. Liu, D. D. Grimes, Y.-W. Lin, A. H. Gheorghe, R. Vexiau, N. Bouloufa-Maafa, O. Dulieu,

- T. Rosenband, and K.-K. Ni, Direct observation of bimolecular reactions of ultracold KRb molecules, *Science* **366**, 1111 (2019).
- [30] P. Gersema, K. K. Voges, M. Meyer zum Alten Borgloh, L. Koch, T. Hartmann, A. Zenesini, S. Ospelkaus, J. Lin, J. He, and D. Wang, Probing photoinduced two-body loss of ultracold nonreactive bosonic  $^{23}\text{Na}^{87}\text{Rb}$  and  $^{23}\text{Na}^{39}\text{K}$  molecules, *Phys. Rev. Lett.* **127**, 163401 (2021).
- [31] J. Chang, S. Lee, Y. Kim, Y. Lim, and J. W. Park, Dual-species bose-einstein condensates of  $^{23}\text{Na}$  and  $^{41}\text{K}$  with tunable interactions, *Phys. Rev. Res.* **6**, 013183 (2024).
- [32] K. K. Voges, P. Gersema, T. Hartmann, T. A. Schulze, A. Zenesini, and S. Ospelkaus, Formation of ultracold weakly bound dimers of bosonic  $^{23}\text{Na}^{39}\text{K}$ , *Phys. Rev. A* **101**, 042704 (2020).
- [33] J. Chang, S. Lee, Y. Kim, S. Jang, J. Kim, S. Kim, and J. W. Park, In prep.
- [34] C. Chin, R. Grimm, P. Julienne, and E. Tiesinga, Feshbach resonances in ultracold gases, *Rev. Mod. Phys.* **82**, 1225 (2010).
- [35] A. Derevianko, J. F. Babb, and A. Dalgarno, High-precision calculations of van der waals coefficients for heteronuclear alkali-metal dimers, *Phys. Rev. A* **63**, 052704 (2001).
- [36] A. Viel and A. Simoni, Feshbach resonances and weakly bound molecular states of boson-boson and boson-fermion pairs, *Phys. Rev. A* **93**, 042701 (2016).
- [37] A. Z. Lam, N. Bigagli, C. Warner, W. Yuan, S. Zhang, E. Tiemann, I. Stevenson, and S. Will, High phase-space density gas of nacs feshbach molecules, *Phys. Rev. Res.* **4**, L022019 (2022).
- [38] F. Cinti, D.-W. Wang, and M. Boninsegni, Phases of dipolar bosons in a bilayer geometry, *Phys. Rev. A* **95**, 023622 (2017).
- [39] G. Guijarro, G. E. Astrakharchik, and J. Boronat, Ultradilute quantum liquid of dipolar atoms in a bilayer, *Phys. Rev. Lett.* **128**, 063401 (2022).
- [40] G. Guijarro, G. E. Astrakharchik, G. Morigi, and J. Boronat, Self-assembled chains and solids of dipolar atoms in a multilayer, *Phys. Rev. Lett.* **133**, 233402 (2024).
- [41] M. A. Baranov, M. Dalmonte, G. Pupillo, and P. Zoller, Condensed matter theory of dipolar quantum gases, *Chemical Reviews* **112**, 5012 (2012), pMID: 22877362.
- [42] M. Hans, F. Schmutte, C. Viermann, N. Liebster, M. Sparr, M. K. Oberthaler, and H. Strobel, High signal to noise absorption imaging of alkali atoms at moderate magnetic fields, *Rev. Sci. Instrum.* **92**, 023203 (2021).
- [43] C. Klempt, T. Henninger, O. Topic, M. Scherer, L. Kattner, E. Tiemann, W. Ertmer, and J. J. Arlt, Radio-frequency association of heteronuclear feshbach molecules, *Phys. Rev. A* **78**, 061602 (2008).
- [44] C.-H. Wu, J. W. Park, P. Ahmadi, S. Will, and M. W. Zwierlein, Ultracold fermionic feshbach molecules of  $^{23}\text{Na}^{40}\text{K}$ , *Phys. Rev. Lett.* **109**, 085301 (2012).
- [45] C. Chin and P. S. Julienne, Radio-frequency transitions on weakly bound ultracold molecules, *Phys. Rev. A* **71**, 012713 (2005).